A Finite Element Solution of a Reduced Fokker–Planck Equation*

D. FYFE,[†] A. WEISER,[†] I. BERNSTEIN,[‡] S. EISENSTAT,[†] AND M. SCHULTZ[†]

[†]Department of Computer Science, and[‡]Department of Engineering and Applied Science,
Yale University, New Haven, Connecticut 06520

A linearized Fokker-Planck equation governing the particle loss rate from large magnetic and potential square-well fields is solved using the Rayleigh–Ritz finite element method with tensor-product splines. The results are compared with those obtained from an approximate analytical theory and previous numerical work.

I. INTRODUCTION

A central problem in the study of magnetic-mirror controlled-fusion devices is the determination of particle loss rates. When the joint magnetic–electrostatic trap which provides confinement is deep, the particle distribution function f is almost Maxwell–Boltzmann over most of the single particle phase space. The exception is a boundary layer adjacent to that part of the boundary C which separates trapped particles from untrapped particles. In that region, f is approximated well by the solution of a linerized Fokker–Planck equation (FPE) which is elliptic and self-adjoint. The particle loss rate is then given by an integral of f.

The boundary curve C and the coefficients in the Fokker–Planck equation are sufficiently complex that no exact analytic solutions are known. For the limiting case of a square-well trap, Pastukhov [1] found an analytic approximate solution by replacing the actual loss boundary by one that matched it locally in the region which makes the dominant contribution to the loss rate. Cohen et al. [2] extended this approximate solution to apply to either ions or electrons in arbitrary wells via a bounce-averaged Fokker–Planck equation. Cohen et al. [2] also solved the problem numerically for square-well fields in order to ascertain the validity of the analytic approximate solutions, solving the time-dependent nonlinear Fokker–Planck equation with a source of low-energy particles until a steady-state was reached.

In this paper we describe a finite element approach to the problem. In Section II,

327

we present a mathematical description. In Section III, we describe the Rayleigh–Ritz finite element method used to numerically solve the linearized Fokker–Planck equation. Finally, in Section IV, we compare our results with those obtained in [2].

II. The Problem

Cohen *et al.* [2] have given the high-velocity limit of the Fokker–Planck equation for a single species of ions of mass m and charge Z confined by a large ambipolar potential. If $F \equiv f/f_M$, where f is the distribution function and $f_M \equiv N(m/2\pi T)^{3/2} e^{-mv^2/2T}$ is the background Maxwellian corresponding to density N and temperature T, then the Fokker–Planck equation is given by

$$\frac{\partial f}{\partial t} + \mathbf{v} \cdot \nabla f + \frac{Ze}{m} \left(\mathbf{E} + \frac{1}{c} \mathbf{v} \times \mathbf{B} \right) \cdot \nabla_v f = \nabla_v \cdot \left[(\nabla_v f) \cdot \nabla_v \nabla_v g - 2f \nabla_v h \right]. \quad (1)$$

If the magnitudes of the magnetic field and the electrostatic potential are modeled as square wells, then the quasi-static approximate equation is given by

$$L(F) \equiv \frac{\partial}{\partial X} \left[p(X, Y) \frac{\partial F}{\partial X} \right] + \frac{\partial}{\partial Y} \left[q(X, Y) \frac{\partial F}{\partial Y} \right] = 0, \quad (2)$$

where

$$p(X, Y) \equiv e^{-X} \quad (3a)$$

and

$$q(X, Y) \equiv \frac{(1 - Y^2) e^{-X}}{4X}; \quad (3b)$$

$X = mv^2/2T$ is a dimensionless energy; $Y = (\mathbf{v} \cdot \mathbf{B})/(vB)$ is the cosine of the pitch angle; $v_{th} = (T/m)^{1/2}$ is the ion thermal speed; $\omega_p = (4\pi NZ^2e^2/m)^{1/2}$ is the ion plasma frequency; and Λ_c is the Coulomb logarithm.
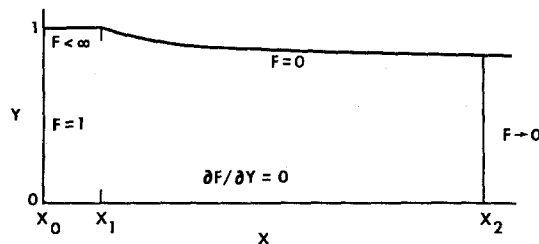

FIG. 1.   The domain of large velocities where the reduced Fokker–Planck equation (2) applies.

Equation (2) is valid in the region

$$D : X > X_0, \qquad 0 < Y < \mathrm{MIN}\{1, z(X)\}, \qquad \text{where} \quad z(X) = \left[1 - \frac{1}{R} + \frac{X_1}{RX}\right]^{1/2}, \quad (4)$$

shown in Fig. 1 and is subject to the following boundary conditions:

$$\text{BC1:} \quad F(X_0, Y) = 1, \qquad \text{for} \quad 0 \leqslant Y \leqslant 1; \tag{5a}$$

$$\text{BC2:} \quad \frac{\partial F}{\partial Y}(X, 0) = 0, \qquad \text{for} \quad X_0 \leqslant X; \tag{5b}$$

$$\text{BC3:} \quad F(X, 1) < \infty, \qquad \text{for} \quad X_0 \leqslant X \leqslant X_1; \tag{5c}$$

$$\text{BC4:} \quad F(X, z(X)) = 0, \qquad \text{for} \quad X_1 \leqslant X; \tag{5d}$$

$$\text{BC5:} \quad e^{-X}F \to 0, \qquad \text{as} \quad X \to \infty. \tag{5e}$$

Here $X_1 \equiv Ze\phi/T$ is the difference in the confining potential between the throat and the center, in units of the background temperature T, and $R \equiv (B \text{ at throat})/(B \text{ at center})$ is the mirror ratio at the throat. The boundary condition BC1 states that the distribution function in the region near the loss boundary should asymptotically match the Maxwellian at low velocities; the value of the dimensionless energy X_0 where this matching takes place is as yet undetermined. The boundary condition BC2 expresses the symmetry of the distribution function about the velocity–space midplane. The boundary condition BC3 is a regularity condition for the distribution function at low velocities and zero pitch angle. The boundary condition BC4 expresses the vanishing of the distribution function at the loss boundary. Finally, the boundary condition BC5 states that the distribution function should approach zero at large velocities.

Equation (2) is the Euler equation of the variational integral

$$V(F) \equiv \int_D \left[p \left(\frac{\partial F}{\partial X}\right)^2 + q \left(\frac{\partial F}{\partial Y}\right)^2 \right] dX\, dY. \tag{6}$$

Any continuously differentiable function $F(X, Y)$ which satisfies the essential boundary conditions BC1, BC4, and BC5 and minimizes $V(F)$ over the set of all such functions also satisfies (2) and the natural boundary conditions BC2 and BC3.

If Eq. (1) is integrated over the trapped particle domain in **v** space, then applying Gauss' theorem to the collision term on the right-hand side gives

$$P = \int \mathbf{n} \cdot [(\nabla_v f) \cdot \nabla_v \nabla_v g - 2f \nabla_v h]\, dA, \tag{7}$$

for the particle flux across the loss boundary, where the integral is over the surface of

the loss region and $\mathbf{n}$ is the outward normal to the surface. In the quasi-static high-velocity approximation this becomes

$$
\begin{aligned}
P &= \frac{\omega_p^4 A_c}{(2\pi)^{3/2} v_{th}^3} \left[\int_{X_1}^{\infty} q(X, z(X)) \frac{\partial F}{\partial Y}(X, z(X))\, dX \right. \\
&\quad \left. + \int_{(1-1/R)^{1/2}}^{1} p(z^{-1}(Y), Y) \frac{\partial F}{\partial X}(z^{-1}(Y), Y)\, dY \right] \\
&= -\frac{\omega_p^4 A_c}{(2\pi)^{3/2} v_{th}^3} \int_0^1 \frac{\partial F}{\partial X}(X_0, Y)\, dY,
\end{aligned}
\tag{8}
$$

where the last equality is obtained by integrating (2) over the domain D. By multiplying (2) by F, integrating by parts, and applying the boundary conditions (5), one can show that

$$
P = \frac{\omega_p^4 A_c}{(2\pi)^{3/2} v_{th}^3} V(F),
\tag{9}
$$

i.e., the particle loss rate is proportional to the minimum of the variational integral $V(F)$ over the set of smooth functions satisfying the essential boundary conditions.

III. THE NUMERICAL METHOD

In this section, we describe a Rayleigh–Ritz finite element method for finding an approximate solution to (2)–(5). In contrast to a finite difference method which would approximate the value of the solution F on some grid, a finite element method finds an approximation to F from a finite-dimensional affine subspace of the affine space S of smooth functions which satisfy the essential boundary conditions. We begin with a general discussion of the Rayleigh–Ritz method.

Let $g(X, Y)$ be any smooth function which satisfies the essential boundary conditions BC1, BC4, and BC5; let S_0^h be a finite-dimensional linear space of functions $u(X, Y)$ satisfying BC4, BC5, and

$$
\text{BC1}': \quad F(X_0, Y) = 0, \qquad \text{for} \quad 0 \leqslant Y \leqslant 1;
\tag{5a'}
$$

and let $\{B_k(X, Y)\}$ be a basis for S_0^h. Then the Rayleigh–Ritz approximation to the solution of (2)–(5) from the affine subspace $g + S_0^h$ is given by

$$
F_h(X, Y) = g(X, Y) + \sum_k d_k B_k(X, Y),
\tag{10}
$$

where the coefficients d_k are chosen to minimize $V(F_h)$:

$$
V(F_h) = \underset{u \in S_0^h}{\text{MIN}}\, V(g + u).
\tag{11}
$$

Setting the first variation of $V(F_h)$ to zero, we find that

$$\sum_j a_{ij} d_j = r_i,$$ (12a)

where

$$a_{ij} \equiv \int_D \left[p \frac{\partial B_i}{\partial X} \frac{\partial B_j}{\partial X} + q \frac{\partial B_i}{\partial Y} \frac{\partial B_j}{\partial Y} \right] dX \, dY$$ (12b)

and

$$r_i \equiv - \int_D \left[p \frac{\partial B_i}{\partial X} \frac{\partial g}{\partial X} + q \frac{\partial B_i}{\partial Y} \frac{\partial g}{\partial Y} \right] dX \, dY.$$ (12c)

Note that F_h satisfies BC1, BC2, and BC5 exactly. Recalling that F minimizes $V(F)$ over the affine subspace S of all smooth functions which satisfy these essential boundary conditions, it follows that $V(F_h) \geqslant V(F)$, i.e., that the estimate for the particle flux will be conservatively high. Moreover, it can be shown that

$$V(F_h) - V(F) \leqslant K \, \underset{u \in S_0^h}{\text{MIN}} \, |F - (g + u)|_{1,2}^2,$$ (13)

where K is some constant independent of S_0^h and

$$|u|_{1,2}^2 \equiv \int_D \left[\left(\frac{\partial u}{\partial X} \right)^2 + \left(\frac{\partial u}{\partial Y} \right)^2 \right] dX \, dY,$$ (14)

so that the error in the flux approximation is proportional to the square of the error in the derivatives of the approximation (see [3]). Finally, since the Rayleigh–Ritz approximation minimizes V over the affine subspace $g + S_0^h$, $V(F_h)$ decreases monotonically toward $V(F)$ as S_0^h grows.

Problem (2)–(5) is posed on an infinite domain which introduces complications for a numerical method. Thus we truncate the domain at some sufficiently large $X = X_2$ and replace the boundary condition BC5 by

$$\text{BC5}': \quad \frac{\partial F}{\partial X} (X_2, Y) = 0, \qquad \text{for} \quad 0 \leqslant Y \leqslant z(X)$$ (5e')

(n.b., BC5' is *not* an essential boundary condition as was BC5).

Finding basis functions which satisfy the essential boundary conditions BC1' and BC4 is made difficult by the curved loss boundary (cf. [2]). To avoid this problem, we transform the domain into a rectangle by the mapping

$$x(X, Y) \equiv X,$$ (15a)

$$y(X, Y) \equiv Y, \qquad X_0 \leqslant X \leqslant X_1,$$
$$\equiv Y/z(X), \qquad X_1 \leqslant X.$$ (15b)

Note that the transformation has discontinuous X-derivatives at $X = X_1$ which means that the solution to the transformed problem will have discontinuous derivatives as well.

Having reduced the irregular, semi-infinite domain D to a rectangle, we choose the functions in S_0^h to be products of piecewise polynomials. The B-splines are a very flexible basis for univariate piecewise polynomials of arbitrary order and continuity on a (nonuniform) mesh (see [4]). The particular space is determined by the order (= degree plus one) and a set of knots which specify where the breaks between piecewise polynomials occur and (by their multiplicity) the number of continuous derivatives at such points. Let the space S^h be the span of all products of the form $b_i^x b_j^y$, where the $\{b_i^x\}$ and $b_j^y\}$ are the univariate B-splines defined on the intervals $[X_0, X_2]$ and $[0, 1]$, respectively. We take S_0^h as the subspace of functions in S^h which satisfy the essential boundary conditions BC1' and BC4.

Recall that the solution to the transformed problem has a discontinuous x-derivative at $x = X_1$. Thus we must include functions which satisfy this condition in the subspace S_0^h. This is easily done by putting a multiple knot at that point.

Also F seems to have singular derivatives near the loss boundary vertex, and we would like to grade the mesh nearby so as to achieve higher accuracy in the approximate solution. But again nonuniform meshes are easily handled by B-splines. We used a β-graded mesh (see [5]), e.g., the mesh

$$x(i) = (i/N)^\beta, \qquad 0 \leqslant i \leqslant N, \tag{16}$$

on $[0, 1]$, where β is a positive constant. The proper choice of β ensures that the rate of convergence for singular problems (as a function of the dimension of S_0^h) is the same as that for nonsingular problems (see [6]).

Up to now, we have not specified $g(X, Y)$ and have been somewhat vague on how to find the subspace of S^h which satisfies the essential boundary conditions BC1' and BC4. Both of these problems can be handled in the same fashion. We fix the coefficients of a basis for those functions in S^h which do not satisfy BC1' and BC4 by doing a least-squares projection of the boundary data; i.e., we choose the coefficients to minimize

$$\int_S [g - h(s)]^2 \, ds, \tag{17}$$

where S denotes that part of the boundary where the essential boundary conditions are posed and h denotes the value of the solution on S. This means solving the linear system

$$\sum_j b_{ij} d_j = t_i, \tag{18a}$$

where

$$b_{ij} \equiv \int_S B_i B_j \, ds, \tag{18b}$$

$$t_i \equiv \int_S B_i h(s) \, ds, \tag{18c}$$

and i and j run over the indices of those basis functions which do not satisfy BC1′ and BC4. Since the boundary values are constant, there exist functions in S_h which satisfy the essential boundary conditions exactly and the corresponding g will as well.

Instead of solving (18) separately and then forming and solving the Rayleigh–Ritz equations, we use a penalty method. First we form the Rayleigh–Ritz equations as if there were no essential boundary conditions, using the entire space S^h. Then we add in a large multiple of the least-squares equations. A careful analysis (see [7]) shows that in essence we are solving for g and the Rayleigh–Ritz approximation $g + S_0^h$ simultaneously.

The coefficient matrix of the linear system is symmetric and positive-definite, and the natural ordering of basis functions yields a ragged band of nonzero entries. We use a profile Cholesky algorithm (see [8]) to solve for F_h.

Up to now, we have formulated everything in terms of integrals, but in practice such integrals must be computed numerically. We used a tensor-product Gauss–Legendre quadrature both to form the Rayleigh–Ritz equations (see [9]) and to evaluate the flux. In small- to medium-sized problems, the cost of evaluating these integrals dominates the cost of solving the linear system so that efficient assembly is crucial. By integrating first in x and then in y, it is possible to significantly improve the efficiency of the assembly phase (see [6, 10]).

IV. RESULTS

The affine space S_h is determined by the input parameters X_0, X_1, X_2, R; the number (NXL) of mesh intervals in x between X_0 and X_1; the number (NXU) of mesh intervals in x between X_1 and X_2; the number (NY) of mesh intervals in y; the order (K) and continuity (C) of the basis functions; and the β-grading factors (β_x and β_y) in x and y. The numerical solution also depends on the number of quadrature points per rectangular mesh element used for setting up the Rayleigh–Ritz equations (NQS) and for evaluating the flux (NQF).

TABLE I

Black Box Parameter Settings

Parameter:	$X0$	NXL	NXR	NY	K	C	β_x	β_y	NQS	NQF
Value:	$X1/8$	4	8	8	4	2	4	4	3	5

TABLE II

Typical Tensor-Product Mesh ($X_1 = 3$, $R = 10$)

X-axis mesh	Y-axis mesh
0.3750000	0.0000000
1.6190060	0.2369535
2.6889985	0.4739070
2.9805624	0.7107501
3.0000000	0.8815232
3.0194376	0.9625132
3.3110015	0.9925952
4.3809940	0.9995372
5.6250000	1.0000000
7.4910090	
10.2900220	
14.4885430	
20.7863230	

Since X_1 and R are the only physical input parameters, it is desirable to fix the remaining parameters and to consider the code as a black box returning a flux approximation $P(X_1, R)$ which depends only on X_1 and R. For the particular case $X_1 = 3$ and $R = 10$, we found that $P(X_1, R)$ was relatively insensitive to changes in the parameter settings given in Table I; refining any of these parameters produced changes in the particle flux of less than 1 part in 100. Basically, the code uses C^2-bicubic splines which may have jumps in the x-derivative at X_1; the B-spline break points for this case are given in Table II (the last four mesh intervals in x were chosen to increase geometrically by a factor of $\frac{3}{2}$). Fortunately, we found these parameter settings were also satisfactory for other values of interest for X_1 and R.

For the problem as formulated in Eqs. (2)–(5), the flux estimates were somewhat higher than the flux estimates reported in [2]. When the asymptotic Rosenbluth potentials appearing in the coefficients were replaced by their isotropic counterparts, i.e., the coefficients in (2) were taken to be

$$p(X, Y) \equiv e^{-X}[\mathrm{erf}(X^{1/2}) - X^{1/2}e^{-X}] \tag{3a'}$$

and

$$q(X, Y) \equiv e^{-X} \frac{(1 - Y^2)}{4X} \left[\left(1 - \frac{1}{2X}\right) \mathrm{erf}(X^{1/2}) - \frac{1}{2} X^{-1/2}e^{-X} \right], \tag{3b'}$$

agreement with the estimates in [2] was within a few percent for many values of interest for X_1 and R.

Results for selected confining potentials and mirror ratios are shown in Figs. 2 and 3, comparing estimates for the confinement time τ ($= N/P$) to the numerical estimates obtained by Cohen et al. and the analytic approximation due to Pastukhov [2].
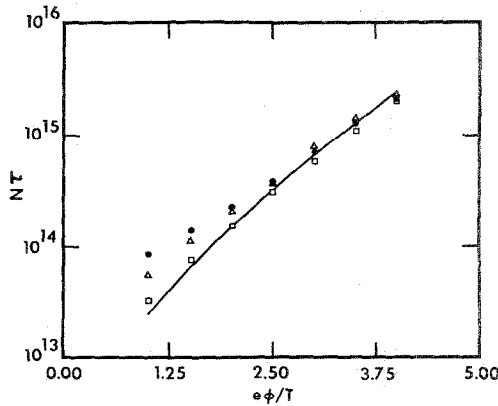
FIG. 2. Ion confinement time versus potential for $R = 10$, $T = 30\,\text{keV}$, $m = 2.5\,\text{amu}$, $Z = 1$. The solid curve is the analytic approximation due to Pastukhov; the points labeled $\triangle$ are the numerical estimates obtained by Cohen et al.; the points labeled $\square$ are the results for the asymptotic Rosenbluth potentials; and the points labeled $\bullet$ are the results for the isotropic Rosenbluth potentials.

Figure 2 is a plot of the confinement time versus the potential for a single ion species of mass $m = 2.5\,\text{amu}$, temperature $T = 30\,\text{keV}$, $Z = 1$, and mirror ratio $R = 10$. For large potentials, the agreement with previous work is good. The deviation at small potentials is probably due to the fact that (2) is only valid for large potentials.

Figure 3 is a plot of the confinement time versus the mirror ratio for a single ion species of mass $m = 2.5\,\text{amu}$, temperature $T = 30\,\text{keV}$, $Z = 1$, and confining potential $e\phi/T = 3$. For small mirror ratios, the agreement with previous work is again good.
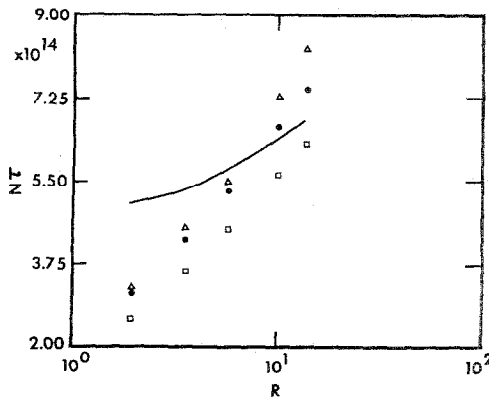

FIG. 3. Ion confinement time versus mirror ration for $e\phi/T = 3$, $T = 30\,\text{keV}$, $m = 2.5\,\text{amu}$, $Z = 1$. The solid curve is the analytic approximation due to Pastukhov; the points labeled $\triangle$ are the numerical estimates obtained by Cohen et al.; the points labeled $\square$ for the asymptotic Rosenbluth potentials; and the points labeled $\bullet$ are the results for the isotropic Rosenbluth potentials.

The deviation at large mirror ratios may be due to differences in the handling of the loss boundary.

In comparing these results, it is important to bear in mind that Eq. (2) is only an approximation to Eq. (1). Pastukhov gave an approximate analytic solution to (2); and the results presented here are an accurate numerical solution. On the other hand, the results of Cohen *et al.* were obtained by solving numerically the time-dependent nonlinear Fokker–Planck equation (1) by methods appropriate for a more complex problem, but correspondingly less accurate than those used in this work.

In summary, the large-potential, high-velocity reduced Fokker–Planck equation exhibits many of the difficulties typically encountered in solving linear elliptic boundary-value problems. Given a proper formulation, the use of finite element methods with tensor-product basis functions was confirmed as a robust and efficient numerical method for the solution of such problems. In particular, the inability to satisfy essential boundary conditions exactly, which could have been a nagging source of error, was avoided by mapping the original domain into a rectangle,[1] a technique which applies to nonlinear and time-dependent poblems as well; and the lack of smoothness of the solution to the mapped problem was handled by semi-local mesh refinement and the use of nonsmooth basis functions.

REFERENCES

1. V. P. PASTUKHOV, *Nucl. Fusion* **14** (1974), 3.
2. R. H. COHEN, M. E. RENSINK, T. A. CUTLER, AND A. A. MIRIN, *Nucl. Fusion* **18** (1978), 1229.
3. S. G. MIKHLIN, "Variational Methods in Mathematical Physics," Macmillan Co., New York, 1964.
4. C. DEBOOR, "A Practical Guide to Splines," Springer-Verlag, New York, 1978.
5. J. R. RICE, *in* "Approximations with Special Emphasis on Spline Functions" (I. J. Schoenberg, Ed.), pp. 349–367, Academic Press, New York, 1969.
6. S. C. EISENSTAT, AND M. H. SCHULTZ, *in* "Mathematical Foundations of the Finite Element Method with Applications to Partial Differential Equations" (A. K. Aziz, Ed.), pp. 505–524, Academic Press, New York, 1972.
7. C. L. LAWSON, AND R. J. HANSON, "Solving Least Squares Problems," Prentice–Hall, Englewood Cliffs, N.J., 1974.
8. A. JENNINGS, *Comput. J.* **9** (1967), 281.
9. G. J. FIX, *in* "Mathematical Foundations of the Finite Element Method with Applications to Partial Differential Equations" (A. K. Aziz, Ed.), pp. 525–556, Academic Press, New York, 1972.
10. A. WEISER, S. C. EISENSTAT, AND M. H. SCHULTZ, *SIAM J. Numer. Anal.* **17** (1980), 908.

[1] In contrast, Cohen *et al.* [2] found possible 10% errors in their estimates of the particle flux for a finite difference approach on the original domain with curved loss boundary, and attributed these errors primarily to the positioning of the grid near the loss boundary.